Hysteresis of Capillary Stress in Unsaturated Granular Soil

William J. Likos, M.ASCE,[1] and Ning Lu, M.ASCE[2]

Abstract: Constitutive relationships among water content, matric suction, and capillary stress in unsaturated granular soils are modeled using a theoretical approach based on the changing geometry of interparticle pore water menisci. A series of equations is developed to describe the net force among particles attributable to the combined effects of negative pore water pressure and surface tension for spherical grains arranged in simple-cubic or tetrahedral packing order. The contact angle at the liquid–solid interface is considered as a variable to evaluate hysteretic behavior in the soil–water characteristic curve, the effective stress parameter χ, and capillary stress. Varying the contact angle from 0 to 40° to simulate drying and wetting processes, respectively, is shown to have an appreciable impact on hysteresis in the constitutive behavior of the modeled soils. A boundary between regimes of positive and negative pore water pressure is identified as a function of water content and contact angle. Results from the analysis are of practical importance in understanding the behavior of unsaturated soils undergoing natural wetting and drying processes, such as infiltration, drainage, and evaporation.

DOI: 10.1061/(ASCE)0733-9399(2004)130:6(646)

CE Database subject headings: Unsaturated soils; Granular materials; Constitutive relation; Dewatering; Hysteresis; Water content.

Introduction

Capillary stress refers to the net interparticle stress generated within a matrix of unsaturated granular particles due to the combined effects of negative pore water pressure and surface tension. The macroscopic consequence of capillary stress is a tendency for the particles to be pulled toward one another, similar in effect and sign convention to an overburden stress or surcharge loading. The important role of capillarity in the shear strength, deformation, and permeability behavior of unsaturated soil has long been recognized. In recent years, analyzing and accounting for capillarity in the context of traditional geotechnical engineering problems including slope stability, bearing capacity, and lateral earth pressure, have become the subjects of much research in the rapidly growing field of unsaturated soil mechanics.

Hysteresis is a well-known phenomenon in many aspects of unsaturated soil behavior. Perhaps, the most outstanding example is the commonly observed hysteresis between drying and wetting loops in the constitutive relationship between soil suction and water content (i.e., the soil–water characteristic curve). Specifically, unsaturated soils undergoing drying processes, such as evaporation or drainage, tend to retain a greater amount of water than at the same magnitude of suction during wetting processes, such as infiltration or capillary rise. Thus, if capillary stress is directly dependent on the magnitude of suction, it follows that there is likely to be some amount of wetting–drying hysteresis in the relationship between capillary stress and water content. In practical engineering situations, where wetting and drying processes occur quite often under natural or imposed changes in environmental conditions, there is a strong motivation to understand this possible hysteretic behavior and the consequent impact on the strength and deformation behavior of unsaturated soil systems.

This paper examines several aspects of hysteretic behavior associated with interparticle pendular pore water menisci and the associated forces acting between and among unsaturated granular soil particles. Relationships among water content, matric suction, Bishop's (1959) effective stress parameter χ, and capillary stress are evaluated by developing a series of analytical equations with the flexibility to account for differences in the contact angle at the solid–water interface. Contact angle is varied from 0 to 40° to simulate drying and wetting processes, respectively, and quantify the associated impact on each of these relationships. Simple-cubic (SC) and tetrahedral (TH) grain packing geometries for idealized uniform spheres are selected as end member scenarios representative of the wide range of fabric in typical soils.

Background Concepts

Capillarity in Unsaturated Soil

Early attempts at understanding capillarity and its role in the engineering behavior of unsaturated soil recognized that when soil is saturated, the pore water pressure is generally positive (compressive) and the net effect of the water pressure is to reduce the effective stress. At the opposite extreme, when the soil is nearly dry, it was recognized that the remaining water in the voids may sustain very high negative pressures, thus creating tensile forces acting to increase the effective stress and pull the soil grains together. Effective stress in the range between these extremes was described in the form of Terzaghi's classic effective stress equation modified to account for the additional contribution from the negative pore pressure, or matric suction (e.g., Bishop 1959, 1961; Donald 1961; Blight 1967).

[1]Assistant Professor, Dept. of Civil and Environmental Engineering, Univ. of Missouri–Columbia, Columbia, MO, 65211. E-mail: likosw@missouri.edu

[2]Associate Professor, Colorado School of Mines, Engineering Division, Golden, CO 80401.

Note. Associate Editor: Majid T. Manzari. Discussion open until November 1, 2004. Separate discussions must be submitted for individual papers. To extend the closing date by one month, a written request must be filed with the ASCE Managing Editor. The manuscript for this paper was submitted for review and possible publication on July 23, 2002; approved on September 2, 2003. This paper is part of the ***Journal of Engineering Mechanics***, Vol. 130, No. 6, June 1, 2004. ©ASCE, ISSN 0733-9399/2004/6-646–655/$18.00.

Bishop's (1959) often cited effective stress approach involves a modified form of Terzaghi's effective stress written as follows:

$$\sigma' = (\sigma - u_a) + \chi(u_a - u_w) \quad (1)$$

where σ'=effective stress; σ=total stress; u_a=pore air pressure; u_w=pore water pressure; and χ=material variable referred to as the ''effective stress parameter'' that is generally believed to vary between zero and unity depending on the degree of pore water saturation. The difference $(\sigma - u_a)$ is referred to as the ''net normal stress'' and the difference $(u_a - u_w)$ is ''matric suction,'' the latter being a positive value if we consider a reference air pressure equal to zero (atmospheric) and the negative pore water pressure typifying unsaturated soil. When χ equals zero (corresponding to perfectly dry conditions) and χ equals unity (corresponding to saturated conditions), Eq. (1) reduces to Terzaghi's classic effective stress equation for describing the behavior of saturated soil $(\sigma' = \sigma - u_w)$. For χ between zero and unity, the second term in Eq. (1), $\chi(u_a - u_w)$, describes the contribution of matric suction to effective stress. Although the validity and practicality of Eq. (1) has been debated for quite some time, it remains a useful macroscopic formulation for describing the important role of interparticle capillary forces on the physical behavior of unsaturated soil.

Understanding capillary stress and its dependency on the degree of saturation in unsaturated soil has historically been a challenging task from both theoretical and experimental perspectives. Previous theoretical investigations, which have for the most part been developed along a particle-scale micromechanical framework, have focused on the complimentary roles of negative pore pressure and surface tension by analyzing the forces resulting from ideally shaped pore water menisci (e.g., toroidal assumption) located between geometrically packed, spherical, or planar particles (e.g., Fisher 1926; Dallavalle 1943; Sparks 1963; Blight 1967; Cho and Santamarina 2001). Additional theoretical models based on free energy minimization formulations under more realistic assumptions of complex nonideal meniscus geometries and additional short-range interaction mechanisms have also been recently explored (Orr et al. 1975; Dobbs and Yeomans 1992; Lian et al. 1993; Molenkemp and Nazemi 2003). Together, these types of models have provided significant insight into the role of capillary forces in governing the particle scale interaction of unsaturated granular particles. Perhaps more importantly, the models have provided a rational conceptual link between the microscale physics that govern the state of stress in unsaturated soil and the numerous macroscopic formulations that have been proposed to describe its engineering behavior [e.g., Eq. (1)]. Very few theoretical studies in the past, however, have investigated hysteretic phenomena in the behavior of interparticle pore water menisci and the consequent capillary stress.

Idealized Grain Geometries

The analysis of water content, pore pressure, and capillary stress in unsaturated soil is greatly simplified by assuming that the grains are perfectly spherical and arranged according to some idealized packing geometry. Figs. 1(a and b) illustrate such geometries for monosized spheres coordinated under SC packing and TH close packing orders, respectively. Unit volumes for the SC and TH packing orders have void ratios of 0.91 and 0.34, respectively, corresponding to porosities of 47.6 and 26.0%. In the following theoretical development, SC and TH packing geometries are considered to represent two end member scenarios in granular soil fabric. It is presumed that the range of water retention and capillary stress behavior of real granular soil falls somewhere between these two idealized cases.

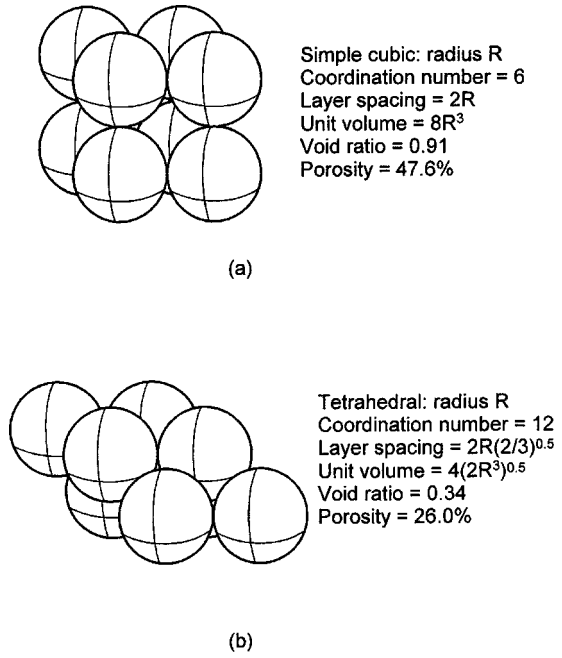

Fig. 1. Idealized grain geometries for uniform spheres in: (a) simple-cubic packing order, and (b) tetrahedral close packing order

Capillary Force between Monosized Contacting Particles

In two dimensions, any two contacting particles can be considered as an elemental volume. Referring to Fig. 2(a), the common radius of the particles is *R*, which for sand or silt grains may range anywhere between approximately 1 mm and 1×10^{-3} mm. Under the assumption of a toroidal meniscus geometry and a rigid system, two additional spherical radii, r_1 and r_2, may be used to fully define the water meniscus, or ''lens,''

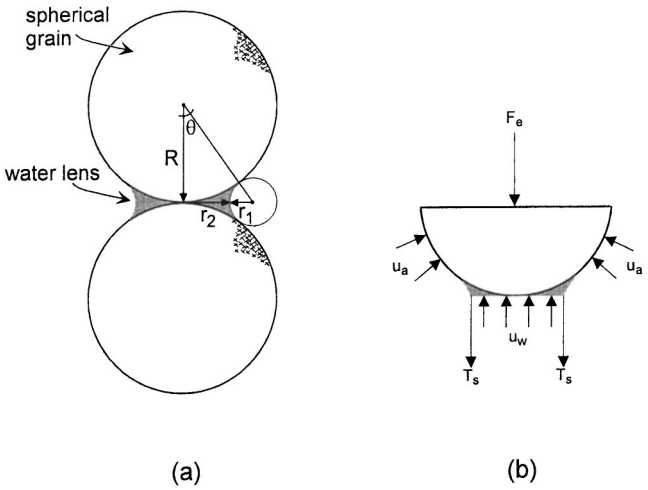

Fig. 2. Water lens between two contacting spheres: (a) radii for describing the lens geometry, and (b) free body diagram for evaluating interparticle forces and stresses

that forms between the particles under unsaturated conditions. The radius r_1, rotated about an axis perpendicular to the cross section shown, defines the concave curvature of the water meniscus. The radius r_2, rotated about an axis parallel to the cross section, defines the convex curvature of the meniscus in the third dimension. The ''filling'' angle θ connects the center of either soil particle to the center of the circle defined by r_1. Increasing or decreasing the filling angle allows changes in the size of the water lens, and thus the water content of the soil–water system, to be described.

The free body diagram for the system, shown in Fig. 2(b), is cut through the center of the water lens at the particle contact point to illustrate the interparticle forces and stresses acting on the unsaturated grains. Isotropic pore air pressure u_a will be upward, resulting in a force on the air–solid interface equal to the following:

$$F_a = u_a(\pi R^2 - \pi r_2^2) \tag{2}$$

At the midplane between the particles, the force due to surface tension along the air–water interface is vertical. The total force due to surface tension is equal to the product of the meniscus circumference and the surface tension of the water T_s, which can be written as follows:

$$F_t = -T_s 2\pi r_2 \tag{3}$$

The projection of total force due to water pressure u_w acting on the water–solid interface in the vertical direction is

$$F_w = u_w \pi r_2^2 \tag{4}$$

The resultant capillary force between the particles is the sum of the above three forces:

$$F_{\text{sum}} = u_a \pi R^2 - u_a \pi r_2^2 + u_w \pi r_2^2 - T_s 2\pi r_2 \tag{5}$$

If the air pressure u_a is the only contribution to the external force, then the capillary force becomes

$$F_e = u_a \pi R^2 - (u_a - u_w)\pi r_2^2 - T_s 2\pi r_2 \tag{6}$$

where the term $(u_a - u_w)$=matric suction. For u_a set to a reference value of zero and for negative pore water pressures, and F_e is a negative number, indicating that the macroscopic effect of capillarity in unsaturated soils is to compress the granular soil matrix, contributing to what has been often referred to as an ''apparent cohesion'' in otherwise cohesionless soils. The second term in the above equation represents the contribution of matric suction to the interparticle capillary force; the third term represents the contribution due to surface tension.

Hysteresis Mechanisms in Unsaturated Soils

The fundamental mechanisms responsible for hysteresis between wetting and drying loops in unsaturated soil behavior are not well understood. The phenomenon has been generally attributed to numerous mechanisms, including: (1) the effects of nonhomogeneous pore size distribution, often referred to as the ''inkbottle'' effect, (2) capillary condensation, which is related to adsorbed water films on the surfaces of fine-grained particles, (3) entrapped air, which refers to the formation of occluded air bubbles during wetting, (4) swelling and shrinkage, which may alter soil fabric differently during wetting and drying, and (5) contact angle hysteresis, which is related to the difference between drying and wetting contact angles at the solid (i.e., soil particle) and liquid (i.e., pore water) interface (e.g., Israelachvili 1992; Iwata et al. 1995).

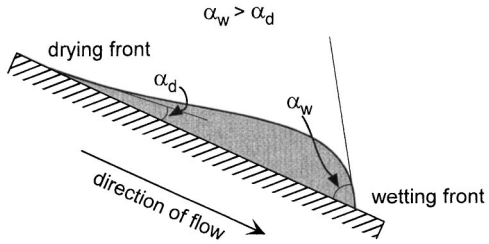

Fig. 3. Water drop on a tilted surface illustrating hysteresis between wetting and drying (advancing and receding) contact angles

The relative importance of the specific hysteresis mechanisms remains unclear. However, in the context of coarse-grained materials, such as sand and silt, surface adsorption mechanisms are probably negligible. Hysteresis in this case is more likely attributable to a combination of the inkbottle effect and contact angle hysteresis. Both mechanisms are scale dependent. For example, one may consider the inkbottle effect as a relatively macroscopic mechanism acting within the pore space defined by the *intraparticle* arrangement of particles and particle groups. On the other hand, contact angle hysteresis is a relatively microscopic mechanism acting on the *interparticle* scale of the individual particles and particle contacts. Due to this disparity in scale, the inkbottle effect is more likely to be important at higher degrees of saturation when the larger pore spaces begin to be filled with water. Similarly, contact angle hysteresis is more likely to be important only at very low water contents when the water is in the form of disconnected menisci between the particle contacts, i.e., the pendular regime. In the following theoretical development, contact angle hysteresis is considered as the primary hysteresis mechanism for granular materials at relatively low water content.

Contact Angle Hysteresis

The three-phase interface between solid particles, pore water, and pore air in unsaturated soils is described by an interfacial contact angle. This angle, designated herein as α, defines the angle measured inside the liquid phase from the solid surface to a point tangent to the liquid–air interface. Contact angles less than 90° indicate a wetting, or hydrophilic, solid–liquid interaction. Contact angles greater than 90° indicate a nonwetting, or hydrophobic, solid–liquid interaction.

Fig. 3 shows a classic example of the contact angle concept for a drop of liquid on an inclined solid surface. As the drop reaches steady-state flow under the influence of gravity, a wetting front characterized by the contact angle α_w, develops at the advancing front of the drop. Similarly, a drying front characterized by the contact angle α_d develops at the receding front of the drop. As shown conceptually in Fig. 3, and in many real solid–liquid–gas interfaces, the wetting contact angle is generally larger than the drying contact angle.

In unsaturated soil–water systems, the difference between wetting and drying contact angles can be significant. Experimental studies based on capillary rise or horizontal infiltration testing, for example, have shown that wetting contact angles in sands can be as high as 60 to 80° (e.g., Letey et al. 1962; Kumar and Malik 1990). Drying contact angles, on the other hand, have been estimated from 0° to as much as 20 to 30° smaller than the wetting angles (e.g., Laroussi and DeBacker 1979).

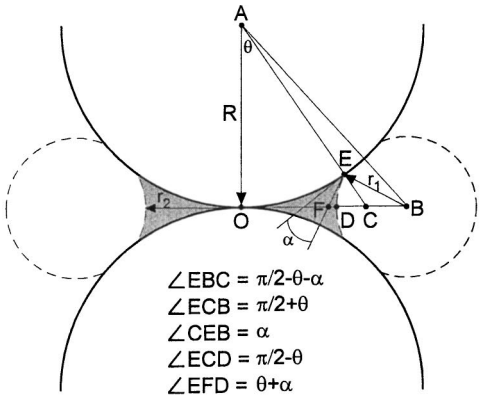

(a)

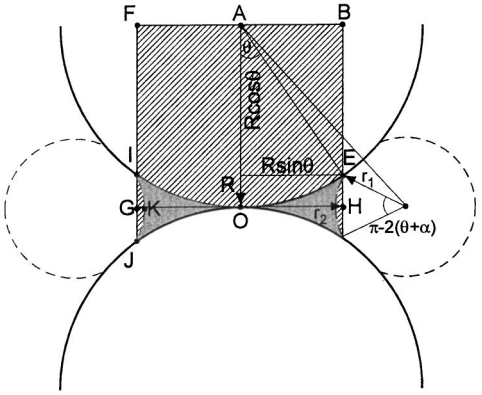

(b)

Fig. 4. Geometrical constraints for defining the water lens between contacting spheres with consideration for a variable contact angle: (a) System radii and angles and (b) surface boundaries in two dimensions

Theoretical Development

Water Content between Two Particles with a Variable Contact Angle

Fig. 4 shows a system geometry for describing the water content between two contacting spherical particles with a variable contact angle. The water lens radii r_1 and r_2 can be written in terms of the filling angle θ, the common particle radius R, and the contact angle α as follows (see Appendix):

$$r_1 = R\frac{1-\cos\theta}{\cos(\theta+\alpha)} \tag{7}$$

$$r_2 = R\tan\theta - r_1\left(1-\frac{\sin\alpha}{\cos\theta}\right) \tag{8}$$

When the contact angle is equal to zero, Eqs. (7) and (8) reduce to the series of equations presented previously by Dallavalle (1943).

In two dimensions, the water lens is bounded by the three hatched surfaces shown in Fig. 4(b). The rectangle $BFGH$, which is a cylinder in three dimensions with a radius of $R\sin\theta$ and height of R, bounds the water lens on the bottom. The partial circle of radius R defined by $FBEOI$ bounds the water lens on the top. The partial circle defined by IKJ bounds the water lens on the sides. Rotated in three dimensions, these surfaces become volumes that can be used to define the total volume of the water lens. The volume of the cylinder $BFGH$ for one unit particle is

$$V_c = 2\pi R^3\sin^2\theta \tag{9}$$

The volume of the partial circle $FBEOI$ for one unit particle is

$$V_s = 2\pi R^3\sin^2\theta\cos\theta + \frac{2\pi}{3}R^3(1-\cos\theta)^2(2+\cos\theta) \tag{10}$$

The volume of the partial circle IJK for one unit particle is

$$V_r = 2\pi\left[r_2 + r_1 - \frac{2}{3}\frac{r_1\cos^3(\theta+\alpha)}{\frac{\pi}{2}-(\theta+\alpha)-\sin(\theta+\alpha)\cos(\theta+\alpha)}\right]$$

$$\times\frac{1}{2}r_1^2[\pi-2(\theta+\alpha)-\sin 2(\theta+\alpha)] \tag{11}$$

Accordingly, the total volume of the water lens is as follows:

$$V_l = (V_c - V_s - V_r) = 2\pi R^3\sin^2\theta - 2\pi R^3\sin^2\theta\cos\theta$$

$$-\frac{2\pi}{3}R^3(1-\cos\theta)^2(2+\cos\theta) - V_r \tag{12}$$

The gravimetric water content for each unit cell of particles in SC packing requires three orthogonal water lenses, and can be expressed as

$$w_{\mathrm{SC}} = \frac{3V_l}{V_{\mathrm{sphere}}G_s} \tag{13}$$

where V_{sphere}=volume of one soil particle (i.e., $V_{\mathrm{sphere}}=4/3\pi R^3$) and G_s=specific gravity of the soil solids. Accordingly, water content can be written in terms of θ and α as

$$w_{\mathrm{SC}} = \frac{9}{2G_s}\sin^2\theta - \frac{9}{2G_s}\sin^2\theta\cos\theta$$

$$-\frac{3}{2G_s}(1-\cos\theta)^2(2+\cos\theta) - \frac{9V_r}{4G_s\pi R^3} \tag{14}$$

In TH packing, the water content is simply twice that of SC packing for the same filling angle:

$$w_{\mathrm{TH}} = 2w_{\mathrm{SC}} \tag{15}$$

Eqs. (14) and (15) are plotted in Fig. 5(a) to demonstrate the relationship between filling angle θ and water content for contact angle α equal to zero. A particle radius of 1 mm and specific gravity equal to 2.65 are selected to represent relatively coarse sand. Previous equations developed by Dallavalle (1943) and Cho and Santamarina (2001), both which assume $\alpha=0°$, are included in Fig. 5(a) for comparison. For $\alpha=0°$, the Dallavalle solution is identical to Eq. (14). The limits of the pendular water regime, and thus the validity of Eqs. (14) and (15), for zero contact angle in SC and TH packing are 0.063 g/g water content and 0.032 g/g respectively (i.e., these are the water contents where individual water lenses from neighboring particles begin to touch each other).

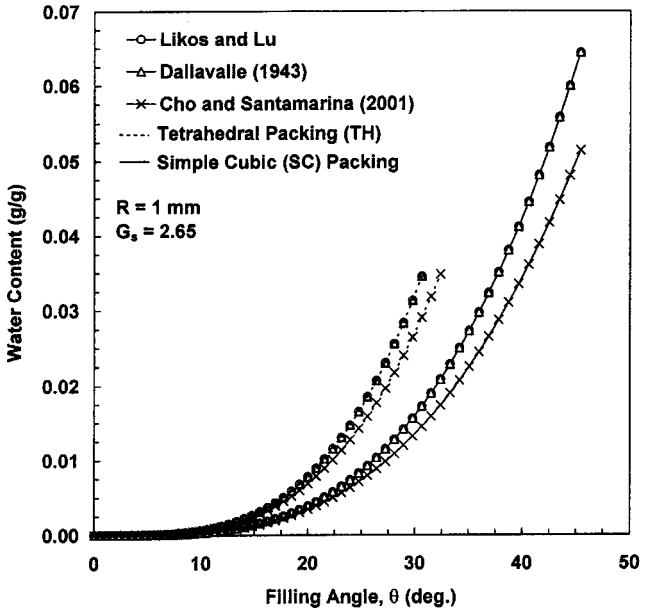

(a)

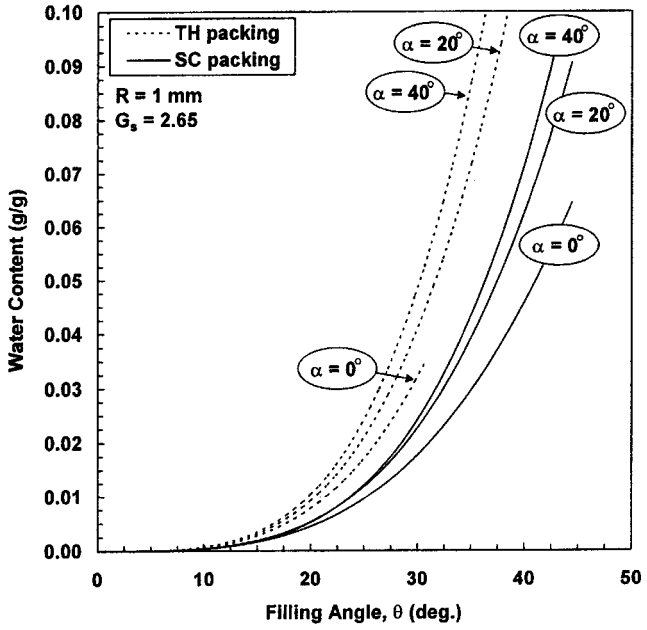

(b)

Fig. 5. Relationship between filling angle θ and gravimetric water content w in simple-cubic and tetrahedral packing: (a) For $\alpha=0°$ and (b) for $\alpha=0°$, $\alpha=20°$, and $\alpha=40°$

Water contents are plotted in Fig. 5(b) for contact angles equal to 0, 20, and 40°. The zero contact angle may be considered representative of drying loop behavior, whereas the nonzero contact angles represent wetting loops. The increase in contact angle has a significant effect on the volume of the water lens and the resultant water content of the soil–water system. Larger contact angles result in higher water contents for a given filling angle θ.

Pore Pressure Regimes

The interplay between contact angle α and filling angle θ has an important role in the boundary between regimes of positive and negative pore pressure. Matric suction for contacting shperes under the toroidal approximation may be written:

$$(u_a-u_w)=T_s\left(\frac{1}{r_1}-\frac{1}{r_2}\right) \tag{16}$$

or, in terms of pore water pressure:

$$u_w=u_a-T_s\left(\frac{1}{r_1}-\frac{1}{r_2}\right) \tag{17}$$

Thus, for u_a equal to zero, Eq. (17) dictates that a decrease in the radius r_1 results in more negative values of pore water pressure, a reflection of its relationship to the concave curvature of the water lens. A decrease in r_2, on the other hand, causes the pore water pressure to be less negative, a reflection of its relationship to the convex curvature of the water lens. If $r_1<r_2$, then pore water pressure less than the air pressure develops in the lens (i.e., a negative value for a reference air pressure equal to zero). If $r_1>r_2$, a positive water pressure develops. Finally, if $r_1=r_2$, which must occur at some value of water content, the pressure in the water lens, and thus the matric suction, are equal to zero. Considering Eqs. (7) and (8), this occurs for contact angle α when the following is true:

$$(1-\cos\theta)(2\cos\theta-\sin\alpha)=\sin\theta\cos(\theta+\alpha) \tag{18}$$

Eq. (18), which is plotted in Fig. 6, identifies the boundary between a negative pore water pressure regime and a positive pore water pressure regime. For example, if $\alpha=0°$, which may represent a drying process, the zero suction condition occurs at $\theta=53.13°$. For $\alpha=60°$, which may represent a wetting process, we have $\theta=20°$. This indicates that positive pressures may develop at much lower water contents for soils undergoing wetting processes.

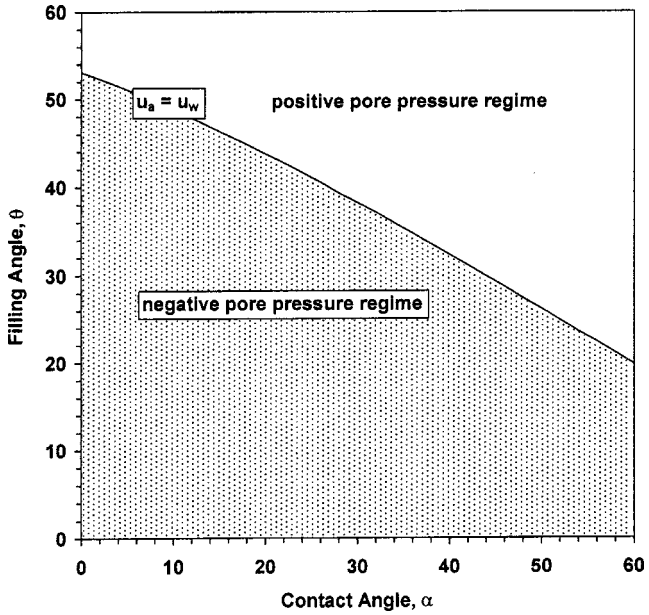

Fig. 6. Relationship between filling angle θ and contact angle α showing boundary between regimes of positive and negative pore–water pressure

Theoretical Soil–Water Characteristic Curves

The preceding development can be used to examine the relationship between matric suction and water content for spherical par-

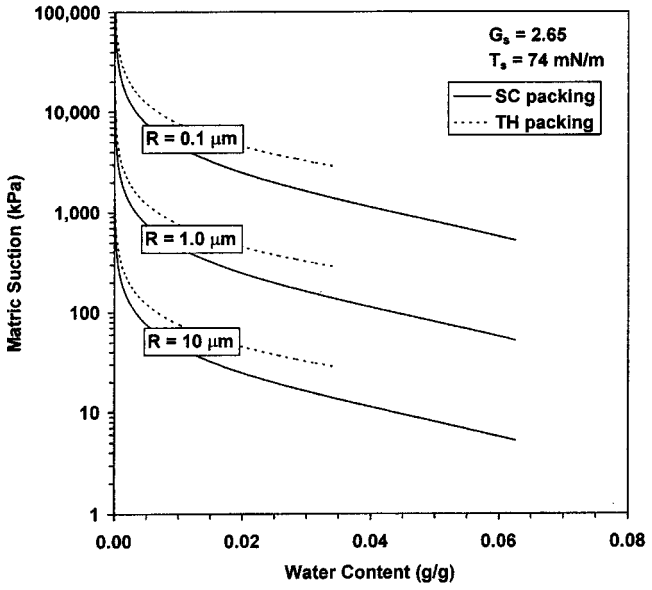

(a)

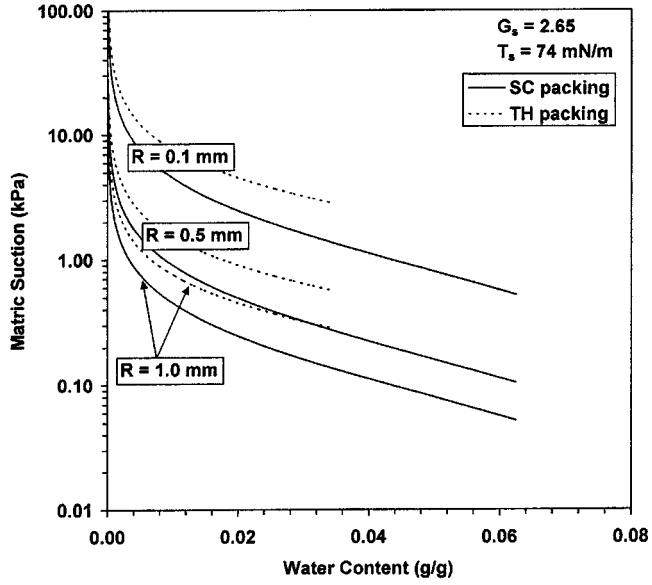

(b)

Fig. 7. Soil–water characteristic curves for various particle sizes in simple-cubic and tetrahedral packing order for (a) relatively fine-grained materials and (b) relatively coarse-grained materials

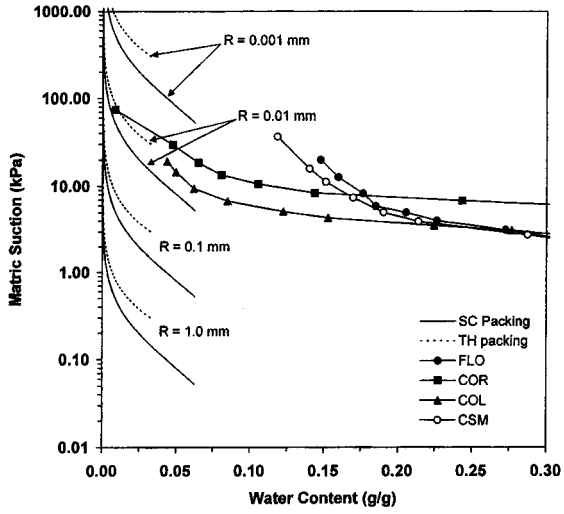

(a)

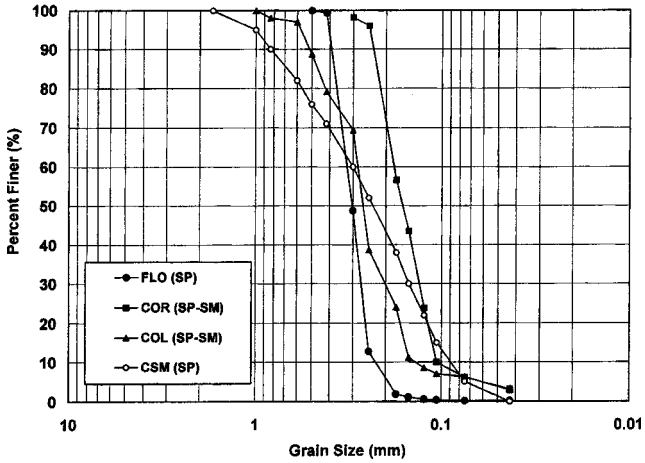

Fig. 8. Theoretical and experimental comparison: (a) theoretical and experimental soil–water characteristic curves, and (b) experimental grain size distribution curves (experimental data from Clayton 1996)

ticles in SC and TH packing order. For θ ranging from 0 to 45°, Eqs. (14) and (15) can be used to calculate water content in SC and TH packing, respectively. Given a fixed particle diameter R and contact angle α, matric suction values corresponding to the calculated water content values can be determined from Eqs. (7), (8), and (16).

Fig. 7 shows soil–water characteristic curves calculated in this manner for six values of R, ranging from 0.1 μm to 1.0 mm, and a zero contact angle. Clearly, the larger the particle size, the less the magnitude of suction for the same value of water content. Fig. 8(a) compares theoretical soil–water characteristic curves for uniform spheres with actual characteristic curves for four sandy specimens measured using a Tempe Cell axis translation apparatus. Fig. 8(b) shows grain size distribution curves for the sands, each indicating a predominant particle size between about 0.5 mm and 0.1 mm. Although there is limited overlap between the modeled water content range and the measured water content range, it appears that the theoretical curves tend to underestimate suction by about 1 to 2 orders of magnitude. The general shape of the experimental curves, however, appears to be reasonably well captured.

Analysis of Hysteresis

Hysteresis in the Soil–Water Characteristic Curve

Fig. 9 shows soil–water characteristic curves for soils modeled with various contact angles. Fig. 9(a) demonstrates curves for two particle radii in SC packing for α equal to 0, 20, and 40°. Fig. 9(b) shows characteristic curves in TH packing order. It is apparent from both figures that the larger contact angles, which may represent a wetting process, result in less water retained by the soils than at the same value of suction for lower contact angles,

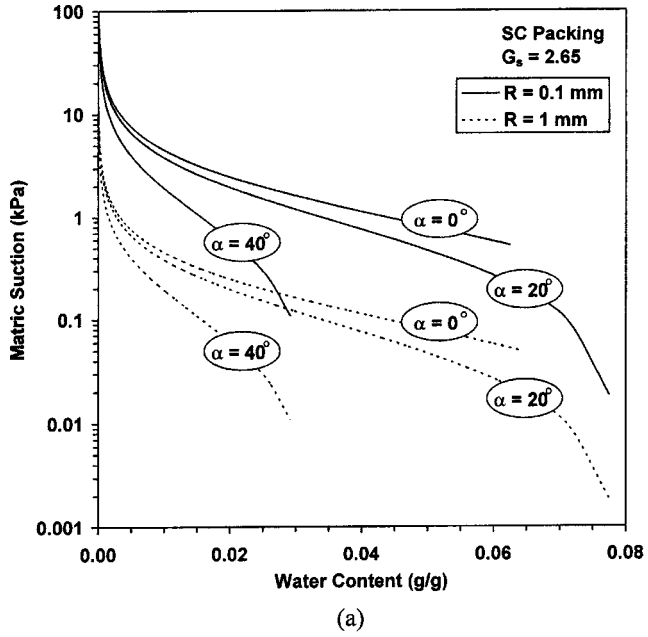

(a)

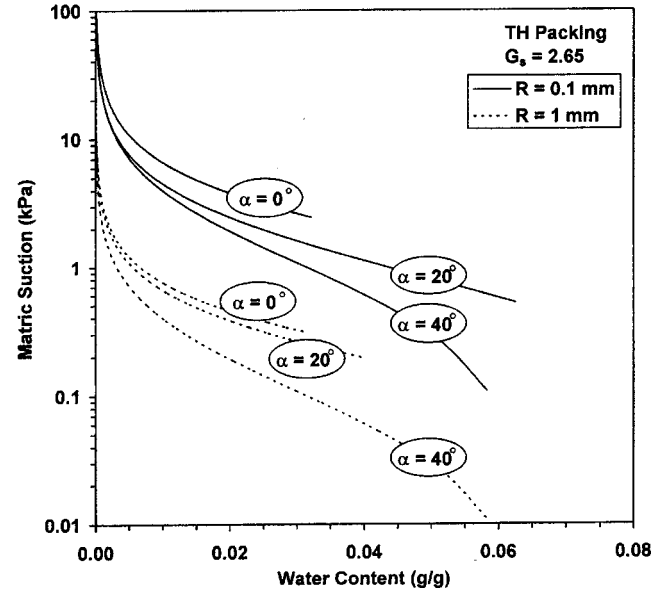

Fig. 9. Effect of contact angle on hysteresis in the soil-water characteristic curve for (a) simple-cubic packing and (b) tetrahedral packing

which may represent a drying process. This trend is identical to that observed in characteristic curves for real soils.

Hysteresis in the Effective Stress Parameter χ

The effective stress owing to capillarity can be evaluated by dividing the interparticle capillary force [Eq. (6)] by the area over which it acts. Taking the cross-sectional area of one particle (πR^2) as a unit area, and employing Eq. (16) to describe surface tension T_s in terms of the radii r_1 and r_2, we can rewrite Eq. (6) in terms of the stress contribution due to capillarity σ_w as follows:

$$\sigma_w = u_a - \frac{r_2^2}{R^2}(u_a - u_w) - \frac{2r_2^2 r_1}{R^2(r_2 - r_1)}(u_a - u_w)$$

$$= u_a - \left[\frac{r_2^2}{R^2} + \frac{2r_2^2 r_1}{R^2(r_2 - r_1)}\right](u_a - u_w)$$

$$= u_a - \frac{r_2^2}{R^2}\frac{r_2 + r_1}{r_2 - r_1}(u_a - u_w) \tag{19}$$

The effective stress under an external total stress σ is

$$\sigma' = \sigma - \sigma_w = \sigma - u_a + \frac{r_2^2}{R^2}\frac{r_2 + r_1}{r_2 - r_1}(u_a - u_w) \tag{20}$$

which is in the same form as Bishop's (1959) single-valued effective stress equation for unsaturated soils, i.e., Eq. (1). If we equate Bishop's equation to Eq. (20), we obtain the following:

$$\sigma - u_a + \chi(u_a - u_w) = \sigma - u_a + \frac{r_2^2}{R^2}\frac{r_2 + r_1}{r_2 - r_1}(u_a - u_w) \tag{21}$$

where

$$\chi = \frac{r_2^2}{R^2}\frac{r_2 + r_1}{r_2 - r_1} \tag{22}$$

In conjunction with Eqs. (7) and (8), Eq. (22) allows us to write the effective stress parameter χ as a function of the filling angle θ and contact angle α as follows:

$$\chi = \left[\tan\theta - \frac{1 - \cos\theta}{\cos(\theta + \alpha)}\frac{\cos\theta - \sin\alpha}{\cos\theta}\right]^2 \times \frac{\tan\theta + \dfrac{1 - \cos\theta}{\cos(\theta + \alpha)}\dfrac{\sin\alpha}{\cos\theta}}{\tan\theta - \dfrac{1 - \cos\theta}{\cos(\theta + \alpha)}\left(2 - \dfrac{\sin\alpha}{\cos\theta}\right)} \tag{23}$$

Eq. (23) provides insightful information into the constitutive relationships among the effective stress parameter χ, water content, and contact angle. Fig. 10, for example, shows the relationship between χ and water content for various contact angles in SC [Fig. 10(a)] and TH [Fig. 10(b)] packing orders. The behavior of the effective stress parameter is independent of particle size. For both SC and TH packing, larger contact angles result in larger values of χ for the same water content.

As shown on Fig. 10(a), the effective stress parameter χ can exceed 1.0, which is contrary to many previous macroscopic experimental studies (e.g., Donald 1956, 1961; Bishop et al. 1960; Blight 1967) but similar to some previous theoretical analysis (e.g., Sparks 1963). Physically, χ greater than 1.0 implies that capillary stress can exceed matric suction. Increasingly large values of χ can be interpreted to reflect the relatively important role of surface tension on the total capillary force [i.e., Eq. (6)]. A recent study by the authors employing a free energy formulation (e.g., Orr et al. 1975) to calculate the exact meniscus geometry shows a $\chi(w)$ function similar to Fig. 10(a), suggesting that the observation of χ greater than 1.0 is not due to the simplified toroidal meniscus geometry approximation. At the present time, experimental evidence of χ greater than 1.0 remains unproven.

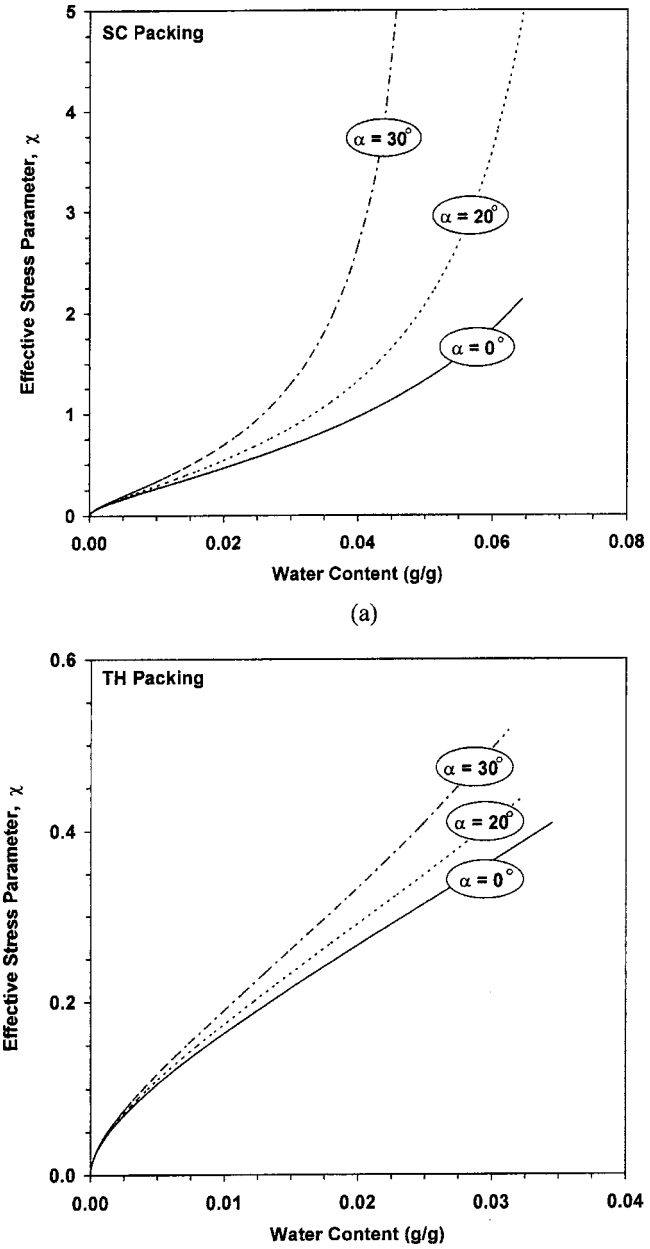

Fig. 10. Theoretical relationship between water content and Bishop's effective stress parameter χ for (a) simple-cubic packing and (b) tetrahedral packing

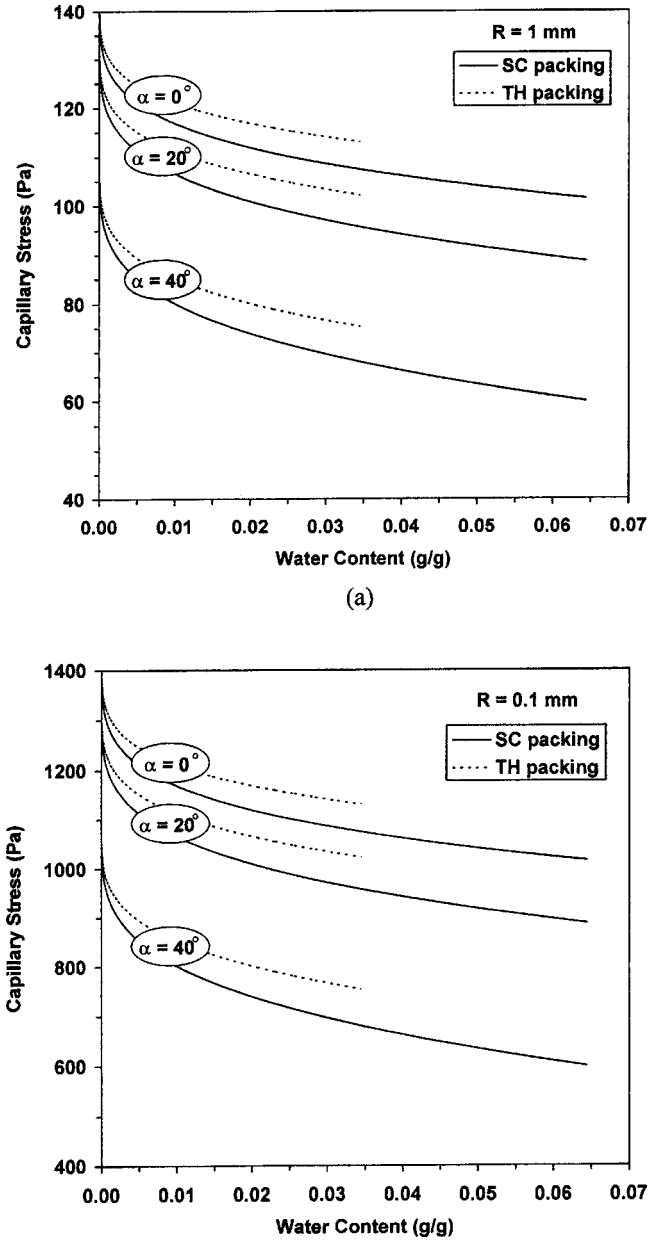

Fig. 11. Relationships among water content, capillary stress, and contact angle in simple-cubic and tetrahedral packing for (a) $R=1$ mm and (b) $R=0.1$ mm

Hysteresis in Capillary Stress

Eq. (19) describes the interparticle stress due to capillarity. Imposing Eq. (16) and setting u_a to a reference value of zero leads to the net capillary stress as a function particle size and the water lens radii r_1 and r_2:

$$\sigma_w = -\frac{r_2^2}{R^2}\left(\frac{r_2+r_1}{r_2-r_1}\right)\left(\frac{r_2-r_1}{r_2 r_1}\right)T_s = -\frac{r_2^2}{R^2}\left(\frac{r_2+r_1}{r_2 r_1}\right)T_s \quad (24)$$

The total capillary force between the two particles is

$$F_{\text{cap}} = \sigma_w \pi R^2 = -\frac{r_2+r_1}{r_1}\pi r_2 T_s \quad (25)$$

Fig. 11 shows the relationship between water content and capillary stress [Eq. (24)] for $R=1$ mm [Fig. 11(a)] and $R=0.1$ mm [Fig. 11(b)]. Capillary stress increases by an order of magnitude with a decrease in particle size of the same order of magnitude. The greater tendency for large capillary forces to develop between relatively fine-grained soils may explain the much greater tendency of fine-grained soils to shrink during drying. Contact angle is varied from 0 to 40° so that the effects of contact angle hysteresis may be evaluated. Increasing the contact angle has a significant effect on the magnitude of capillary stress, i.e., the larger the value of α, the less the capillary stress. This observation may have important practical implications. For example, soils undergoing a wetting process (e.g., an unsaturated slope during a precipitation event) may have a smaller contribution to effective stress from capillarity, and thus less shear strength, than at the same water content during a drying process.

Summary and Conclusions

A theoretical analysis was conducted to model hysteretic behavior in constitutive relationships among water content, matric suction, Bishop's effective stress parameter χ, and capillary stress in unsaturated granular soil. A series of equations was developed to describe the net interparticle forces attributable to negative pore water pressure and surface tension for monosized spherical grains arranged in SC and TH packing order. The contact angle at the liquid–solid interface was considered a material variable in the theoretical development in order to evaluate its influence on hysteresis between cycles of wetting and drying.

Soil–water characteristic curves modeled using the analytical solutions display qualitative behavior similar to real unsaturated soils. Varying the contact angle causes significant hysteresis, where relatively large contact angles (e.g., 40°), selected to model wetting processes, result in significantly lower values of water content for the same suctions obtained for relatively small contact angles (e.g., 0°), selected to model drying processes. A boundary between regimes of positive and negative pore water pressure is identified as a function of water content and contact angle. The results suggest that positive pore pressures in unsaturated soil may occur more readily for wetting processes. The contact angle has a significant impact on the behavior of Bishop's effective stress parameter χ, thus influencing the contribution of matric suction to effective stress. The analysis indicates that χ could be greater than 1.0, which may be a reflection of the relative importance of surface tension as a component of the total capillary force between particles. A solution is developed for describing the magnitude of interparticle capillary stress as a function of water content. Relatively large contact angles result in significantly lower capillary stresses, indicating that the contribution of capillarity to interparticle stress for soils undergoing wetting processes may be less than that for soils undergoing drying processes.

Acknowledgment

Financial support for this study was provided by the National Science Foundation under Grant Nos. CMS-0306823 and DUE-0126306.

Appendix. Derivation of Water Lens Radii, r_1 and r_2

Considering the triangle BCE in Fig. 4(a), the trigonometric theory of sines leads to

$$\frac{r_1}{\sin(\pi/2+\theta)}=\frac{EC}{\sin(\pi/2-\theta-\alpha)}$$
$$EC=\frac{\sin(\pi/2-\theta-\alpha)}{\sin(\pi/2+\theta)}r_1=\frac{\cos(\theta+\alpha)}{\cos\theta}r_1 \quad (26)$$

Considering the triangle AOC and Eq. (26), we have

$$\frac{R}{\cos\theta}-R=EC=\frac{\cos(\theta+\alpha)}{\cos\theta}r_1 \quad (27)$$

Thus, we obtain Eq. (7)

$$r_1=R\frac{1-\cos\theta}{\cos(\theta+\alpha)} \quad (7)$$

Considering the theory of sines for the triangle ECB in Fig. 4(a), we have

$$\frac{r_1}{\sin(\pi/2+\theta)}=\frac{CB}{\sin\alpha}$$
$$CB=\frac{\sin\alpha}{\cos\theta}r_1 \quad (28)$$

Therefore,

$$DC=r_1-CB=r_1\left(1-\frac{\sin\alpha}{\cos\theta}\right) \quad (29)$$

and since

$$r_2=R\tan\theta-DC \quad (30)$$

we arrive at Eq. (8):

$$r_2=R\tan\theta-r_1\left(1-\frac{\sin\alpha}{\cos\theta}\right) \quad (8)$$

References

Bishop, A. W. (1959). "The principle of effective stress." *Tekni. Ukeblad I Samarbeide Med Tekni.*, 106(39), 859–863.

Bishop, A. W. (1961). "The measurement of pore pressure in the triaxial test." *Proc., Conf. on Pore Pressure and Suction in Soils*, Butterworths, London, pp. 38–46.

Bishop, A. W., Alpan, I., Blight, G. E., and Donald, I. B. (1960). "Factors controlling the shear strength of partially saturated cohesive soils." *ASCE Conf. on Shear Strength of Cohesive Soils*, New York, 503–532.

Blight, G. E. (1967). "Effective stress evaluation for unsaturated soils." *J. Soil Mech. Found. Div., Am. Soc. Civ. Eng.*, 92(2), 125–148.

Cho, G. C., and Santamarina, J. C. (2001). "Unsaturated particulate materials—particle-level studies." *J. Geotech. Geoenviron. Eng.*, 127(1), 84–96.

Clayton, W. S. (1996). "Relative permeability–saturation–capillary head relationships for air sparging in soils." PhD dissertation, Colorado School of Mines, Golden, Colo., 282.

Dallavalle, J. M. (1943). *Micromeritics*, Pitman, London.

Dobbs, H. T., and Yeomans, J. M. (1992). "Capillary condensation and prewetting between spheres." *J. Phys.: Condens. Matter*, 4, 10133–10138.

Donald, I. B. (1956). "Shear strength measurements in unsaturated noncohesive soils with negative pore pressures." *Proc., 2nd Australia-New Zealand Conf. on Soil Mechanics and Foundations Engineering*, 200–205.

Donald, I. B. (1961). "The mechanical properties of saturated and partly saturated soils with special reference to negative pore water pressure." PhD dissertation, Univ. of London, London.

Fisher, R. A. (1926). "On the capillary forces in an ideal soil; correction of formula given by W. B. Haines." *J. Agric. Sci.*, 16, 492–505.

Israelachvili, J. (1992). *Intermolecular and surface forces*, 2nd Ed., Academic, New York.

Iwata, S., Tabuchi, T., and Warkentin, B. P. (1995). *Soil–water interactions: Mechanisms and applications*, 2nd Ed., Marcel Dekker, New York.

Kumar, S., and Malik, R. S. (1990). "Verification of quick capillary rise approach for determining pore geometrical characteristics in soils of varying texture." *Soil Sci.*, 150(6), 883–888.

Laroussi, C. H., and DeBacker, L. W. (1979). "Relations between geometrical properties of glass bead media and their main $\psi(\theta)$ hysteresis loops." *Soil Sci. Soc. Am. J.*, 43, 646–650.

Letey, J., Osborn, J., and Pelishek, R. E. (1962). "Measurement of liquid–solid contact angles in soil and sand." *Soil Sci.*, 93, 149–153.

Lian, G., Thornton, C., and Adams, M. J. (1993). ''A theoretical study of the liquid bridge forces between two rigid spherical bodies.'' *J. Colloid Interface Sci.*, 161, 138–147.

Molenkemp, F., and Nazemi, A. H. (2003). ''Interactions between two rough spheres, water bridge, and water vapour.'' *Geotechnique*, 53(2), 255–264.

Orr, F. M., Scriven, L. E., and Rivas, A. P. (1975). ''Pendular rings between solids: Meniscus properties and capillary force.'' *J. Fluid Mech.*, 67(4), 723–742.

Sparks, A. D. W. (1963). ''Theoretical considerations in stress equations for partly saturated soils.'' *Proc., 3rd Regional Conf. for Africa on Soil Mechanics*, Salisbury, Rhodesia, Vol. 1, 215–218.